

# Simultaneous Detection and Tracking with Motion Modelling for Multiple Object Tracking

ShiJie Sun<sup>1</sup>, Naveed Akhtar<sup>2</sup>, XiangYu Song<sup>3</sup>, HuanSheng Song<sup>1</sup>, Ajmal Mian<sup>2</sup>, and Mubarak Shah<sup>4</sup>

<sup>1</sup> Chang'an University, Xi'an, Shaanxi, China  
{shijieSun,hshsong}@chd.edu.cn

<sup>2</sup> University of Western Australia, 35 Stirling Highway, Crawley, WA, Australia  
{naveed.akhtar,ajmal.mian}@uwa.edu.au

<sup>3</sup> Deakin University, RWaurn Ponds, Victoria 3216, Melbourne, Australia  
xiangyu.song@deakin.edu.au

<sup>4</sup> University of Central Florida, Orlando, FL, America  
shah@crcv.ucf.edu

**Abstract.** Deep learning based Multiple Object Tracking (MOT) currently relies on off-the-shelf detectors for tracking-by-detection. This results in deep models that are detector biased and evaluations that are detector influenced. To resolve this issue, we introduce Deep Motion Modeling Network (DMM-Net) that can estimate multiple objects' motion parameters to perform joint detection and association in an end-to-end manner. DMM-Net models object features over multiple frames and simultaneously infers object classes, visibility and their motion parameters. These outputs are readily used to update the tracklets for efficient MOT. DMM-Net achieves PR-MOTA score of 12.80 @ 120+ fps for the popular UA-DETRAC challenge - which is better performance and orders of magnitude faster. We also contribute a synthetic large-scale public dataset Omni-MOT for vehicle tracking that provides precise ground-truth annotations to eliminate the detector influence in MOT evaluation. This 14M+ frames dataset is extendable with our public script (Code at [Dataset](#), [Dataset Recorder](#), [Omni-MOT Source](#)). We demonstrate the suitability of Omni-MOT for deep learning with DMM-Net, and also make the source code of our network public.

**Keywords:** Multiple Object Tracking, Tracking-by-detection, Deep Learning, Simultaneous detection and tracking.

## 1 Introduction

Multiple Object Tracking (MOT) [10], [25], [42], [44] is a longstanding problem in Computer Vision [27]. Contemporary deep learning based MOT has widely adopted the tracking-by-detection paradigm [43], that capitalizes on the natural division of *detection* and *data association* tasks for the problem. In standard MOT evaluation protocol, the object detections are assumed to be known and public detections are provided on evaluation sequences, and MOT algorithms are expected to output object tracks by solving the data association problem.

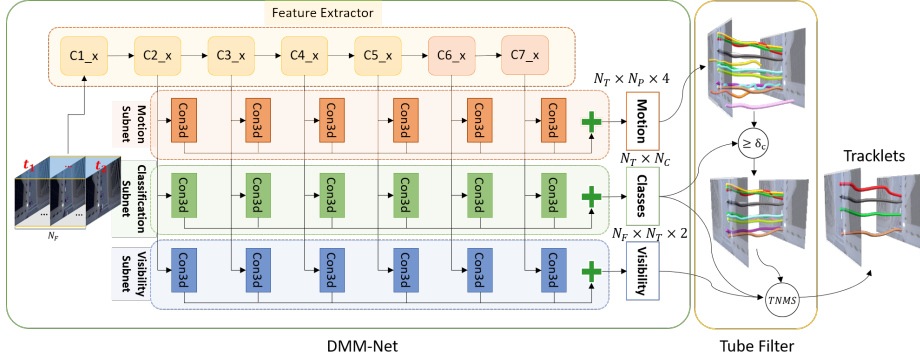


**Fig. 1.** Schematics of the proposed end-to-end trainable DMM-Net:  $N_F$  frames from time stamp  $t_1 : t_2$  are input to the network. The frame sequence is first processed with a *Feature Extractor* comprising 3D ResNet-like [20] convolutional groups. Outputs of the last groups 2 to 7 are processed by Motion Subnet, Classifier Subnet, and Visibility Subnet. Each sub-network uses 3D convolutions to learn features that are concatenated to predict anchor tubes’ motion parameters ( $\mathbf{O}_M \in \mathbb{R}^{N_T \times N_P \times 4}$ ), object classes ( $\mathbf{O}_C \in \mathbb{R}^{N_T \times N_C}$ ), and visibility ( $\mathbf{O}_V \in \mathbb{R}^{N_F \times N_T \times 2}$ ), where  $N_T$ ,  $N_P$  and  $N_C$  denote the number of anchor tubes, motion parameters and object classes (including background). We explain anchor tubes and motion parameters in Section 4. DMM-Net is trained with its specialized loss. For deployment, the anchor tubes predicted by the DMM-Net are filtered to compute tracklets defined over multiple frames. These tracklets are later combined to form a complete track.

Although attractive, using off-the-shelf detectors for MOT also has undesired ramifications. For instance, a deep model employed for the subsequent data association task (or a constituent sub-task) gets biased to the detector. The detector performance can also become a bottle-neck for the overall tracker. Additionally, composite techniques resulting from independent detectors fail to harness the true representation power of deep learning by sacrificing end-to-end training etc. It also seems unnatural that a MOT tracker must be evaluated on different detectors to interpret its tracking performance. All these problems are potentially solvable if trackers can implicitly detect the target objects, and detector bias can be removed from the ground-truth labeling of the tracks. This work makes strides towards these solutions.

We make two major contributions towards setting the tracking-by-detection paradigm free from off-the-shelf detectors in deep learning settings. Our first contribution comes as the first-of-its-kind deep network that performs object detections and data association by estimating multiple object motion parameters in an end-to-end manner. Our network, called Deep Motion Modeling Network (DMM-Net), predicts object motion parameters, their classes and their visibility with the help of three sub-networks, see Fig. 1. These sub-networks exploit feature maps of frames in a video sequence that are learned with a Feature Extractor comprising seven 3D ResNet-like [20] convolutional groups. Instead of individual frames, DMM-Net simultaneously processes multiple (i.e. 16) frames. To handle multiple tracks in those frames, we introduce the notion of anchor

tubes that extends the concept of anchor boxes in object detection [26] along the temporal dimension for MOT. Similar to [26], these anchor tubes are pre-defined to reduce the computation and improve the network speed. The predicted motion parameters can describe the shape offset and scale of each pre-defined anchor tube in the spatio-temporal space. We propose individual losses over the comprehensive representations of the sub-networks to predict object motion parameters, object classes and visibility. The DMM-Net output is readily usable to update the tracks. As our second major contribution, we propose a realistic large-scale dataset with accurate and extensive ground-truth annotations. The proposed dataset, termed Omni-MOT for its comprehensive coverage of the MOT scenarios, is generated with CARLA simulator [13] for vehicle tracking. The dataset comprises 14M+ frames, 250K tracks, 110 million bounding boxes, three weather conditions, three crowd levels and three camera views in five simulated towns. By eliminating the use of off-the-shelf detectors in ground-truth labeling, it removes any detector bias in evaluating the techniques.

The Omni-MOT dataset and DMM-Net source code are both publicly available for the broader research community. For the former, we also provide software tools to freely extend the dataset. We demonstrate the suitability of the Omni-MOT for deep models by training and evaluating DMM-Net on its videos. We also augment DMM-Net with Omni-MOT and evaluate our technique on the popular UA-DETRAC challenge [45]. The remote server computed results show that DMM-Net is able to achieve a very competitive 12.80 score for the comprehensive PR-MOTA metric with the overall speed of 123 fps. The orders of magnitude increase in the speed is directly attributed to the intrinsic detections in our tracking-by-detection technique.

## 2 Related Work

Multiple Object Tracking (MOT) is a fundamental problem in Computer Vision that has attracted significant interest of researchers in recent years. For a general review of the related literature, we refer to Luo et al. [27] and Emami et al. [14]. Here, we focus on the key contributions that relate to this work more closely. With the recent advances in object detectors, tracking-by-detection is fast becoming the common contemporary paradigm for MOT [38], [39], [43], [46]. In this scheme, objects are first detected frame-wise and later associated with each other across multiple frames. Relying on off-the-shelf detectors, techniques following this paradigm mainly focus on object association, which can make them inherently detector biased. These methods can be broadly categorized as local [34], [41] and global [10], [37], [48] approaches. The former use two frames for data association, while the latter associate objects over a larger number of frames.

More recent global techniques cast data association into a network flow problem [4], [7], [33], [40]. For instance, Berclaz et al. [4] solved a constrained flow optimization problem for MOT and used the k-shortest paths algorithm for associating the tracks. Chari et al. [8] added a pairwise cost to the min-cost network flow framework and proposed a convex relaxation of the problem. However, such

methods rely on object detectors rather strongly, which makes them less attractive in the presence of occlusions and misdetections. To mitigate the problems resulting from occlusions, Milan et al. [29] employed a continuous energy minimization framework for MOT that incorporates explicit occlusion reasoning and appearance modeling. Wen et al. [47] also proposed a data association technique based on undirected hierarchical relation hyper-graph.

Sun et al. [42] proposed a deep affinity network to model features of pre-detected objects and compute object affinities by the same network. Bea et al. [3] modified the Siamese Network to learn deep representations for MOT with object association. There are few instances of deep learning techniques that aim at removing the reliance of tracking on independent detectors. For instance, Feichtenhofer et al [15] proposed an R-FCN based network [9] that performs object detection and jointly builds an object model to be used for data association. However, their method is limited to frame-wise detections. Consequently, it only allows frame-by-frame association, requiring manual adjustment of temporal stride. Our technique is inherently different, as it directly computes tracklets over multiple frames by motion modeling, enabling realtime solutions while considering all the frames.

Besides the development of novel techniques, the role of datasets is central to the advancement of deep learning based MOT. Currently, a few large datasets for this task are available, e.g. PETS2009 [17], KITTI [18], DukeMTMC [36], PoseTrack [23], and MOT Challenge datasets [25], [28]. These datasets are recorded in the real world with pedestrians and vehicles as the objects of interest. We refer to the original works for more details on these datasets. Below, we briefly discuss UA-DETRAC [45] for its high relevance to our contribution.

UA-DETRAC [45] is a large dataset for traffic scenes MOT. It provides object bounding boxes, their IDs and information on the overlapped ratio of the objects. However, the provided detections are individually generated by detectors and hence are prone to errors. This results in an undesired detector-bias in tracker evaluation. Besides, different pre-processing procedures of the detectors employed by the dataset also cause problems in fair evaluation. Although UA-DETRAC has served a great purpose in advancing the state-of-the-art in MOT for vehicles, the aforementioned issues call for a more transparent dataset that does not rely on off-the-shelf detectors for evaluating trackers. This work provides such a dataset with realistic settings and complete control over the environment conditions and camera viewpoints.

### 3 Omni-MOT Dataset

We term the proposed dataset as **Omni-MOT** (OMOT) dataset for its comprehensive coverage of the conditions and scenarios possible in MOT. The dataset is publicly available for download. Moreover, we also make the recording script for the dataset public that will enable the community to further extend the data. The provided script has the ability to generate multi-camera videos. The dataset is recorded using virtual cameras in the CARLA simulator [13].

To the best of our knowledge, Omni-MOT is the first realistic large dataset for tracking vehicles that completely relinquishes off-the-shelf detectors in ground truth generation, and provides comprehensive annotations. Moreover, with the provided scripts, the dataset can easily be extended for future research. To put the scale of Omni-MOT into perspective, the provided number of frames is almost 1,200 times larger than MOT17. The number of provided tracks and boxes respectively are 210 and 30 times larger than UA-DETRAC. Not to mention, all the boxes and tracks are simulator generated that avoids any labeling error. Considering that OMOT can also be used for data augmentation, we make the ground truth for the test videos public as well. Please see the supplementary material of the paper for complete details of the dataset.

## 4 Deep Motion Modeling Network

To absolve deep learning based tracking-by-detection from independently pre-trained off-the-shelf detectors, we propose **Deep Motion Modeling Network** (DMM-Net) for online MOT (see Fig. 1). Our network enables MOT by jointly performing object detection, tracking, and classification across multiple video frames without requiring pre-detections and subsequent data association. For a given input video, it outputs objects' motion parameters, classes, and their visibility across the input frames. We provide a detailed discussion of our network below. However, we first introduce the used notations and conventions.

- $N_F, N_C, N_P, N_T$  denote the number of input frames, object classes (0 for 'background'), time-related motion parameters, and anchor tubes.
- $W, H$  are the frame width, and frame height.
- $\mathbf{I}_t$  denotes the video frame at time  $t$ . Subsequently, a 4-D tensor  $\mathbf{I}_{t_1:t_2:N_F} \in \mathbb{R}^{3 \times N_F \times W \times H}$  denotes  $N_F$  video frames from time  $t_1$  to  $t_2 - 1$ . For simplicity, we often ignore the subscript “:  $N_F$ ”.
- $\mathbf{B}_{t_1:t_2:N_F}, \mathbf{C}_{t_1:t_2:N_F}, \mathbf{V}_{t_1:t_2:N_F}$  respectively denote the ground truth boxes, classes and visibilities in the selected  $N_F$  video frames from time  $t_1$  to  $t_2 - 1$ . The text also ignores “:  $N_F$ ” for these notations.
- $\mathbf{O}_{M,t_1:t_2:N_F}, \mathbf{O}_{C,t_1:t_2:N_F}, \mathbf{O}_{V,t_1:t_2:N_F}$  denote the estimated motion parameters, classes, and visibilities. With time stamps and frames clear from the context, we simplify these notations as  $O_M, O_C, O_V$ . In Fig. 2, we illustrate object visibility, classes and motion parameters.

**Conventions:** The shape of a network output tensor is considered to be Batch  $\times$  Channels  $\times$  Duration  $\times$  Width  $\times$  Height, where Duration accounts for the number of frames. For brevity, we often ignore the Batch dimension.

### 4.1 Data Preparation

Appropriate data preparation is important for training (and later testing) our network. In this process, we also avail the opportunity of augmenting the data

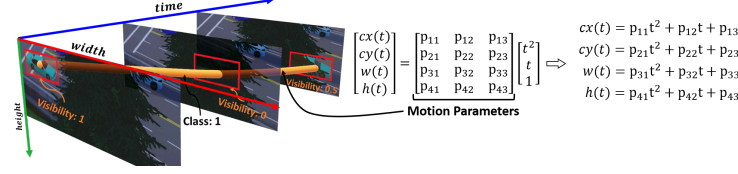


**Fig. 2.** (Best viewed in color) Illustration of motion visibility, class, and motion parameters: The visibility of the vehicle goes from 1 (fully visible) to 0 (invisible) and back to 0.5 (partially visible). Classes are predefined as 1 for vehicle and 0 for everything else. Motion parameters  $\{p_{11}, \dots, p_{43}\}$  are used to locate the center  $x$  ( $cx$ ), center  $y$  ( $cy$ ), width ( $w$ ) and height ( $h$ ) of the tube/tracklet at anytime. We employ a quadratic motion model leveraging  $4 \times 3$  matrices.

**Table 1.** Inputs for training and testing DMM-Net. The tensor dimensions are given as Channels $\times$ Duration $\times$ Width $\times$ Height.  $n_{t_1:t_2}$  is the number of tracks in  $I_{t_1:t_2}$ .

Input	Dimensions/Size	Train	Test
$I_{t_1:t_2}$	$3 \times N_F \times W \times H$	✓	✓
$t_{t_1:t_2}$	$N_F$	✓	✓
$B_{t_1:t_2}$	$N_F \times n_{t_1:t_2} \times 4$	✓	✗
$C_{t_1:t_2}$	$n_{t_1:t_2}$	✓	✗
$V_{t_1:t_2}$	$N_F \times n_{t_1:t_2}$	✓	✗

to induce robustness in our model against camera photometric distortions, background scene variations, and other practical factors. The inputs expected by our network are summarized in Table 1. For training a robust network, we perform the following data pre-processing:

1. *Stochastic frame sequence* is introduced by randomly choosing  $N_F$  frames from  $2N_F$  frames.
2. *Static scene emulation* is done by duplicating selected frames  $N_F$  times.
3. *Photometric camera distortions* are introduced in the frames by scaling each pixel by a random value in the range  $[0.7, 1.5]$ . The resulting frames are converted to HSV format, and their saturation channel is again scaled by a random value in  $[0.7, 1.5]$ . A frame is then converted back to RGB format and re-scaled by a random value in the same range. This process of photometric distortion is inspired by [42].
4. *Frame expansion* is performed by enlarging video frames by a random factor in the range  $[1, 1.2]$ . To that end, we pad the original frames with extra pixels whose value is set to the mean pixel value of the training data.

In our pre-processing, the above-mentioned steps 2-4 are applied to the frames with probability 0.01, 0.5, 0.5, respectively. The resulting frame are then resized to the fixed dimension  $H \times W \times 3$ , and horizontally flipped with a probability of 0.5. We simultaneously process the selected  $N_F$  frames by applying the above mentioned transformations. These RGB video frames are then arranged as 4D-tensors  $I_{t_1:t_2} \in \mathbb{R}^{3 \times N_F \times W \times H}$ . We fill the ground truth data matrices  $B_{t_1:t_2}$ ,  $C_{t_1:t_2}$ ,  $V_{t_1:t_2}$  with the detected boxes, and visibilities in the video frames from  $t_1$  to  $t_2 - 1$ . We set the labeled boxes, classes, and visibilities of fully occluded

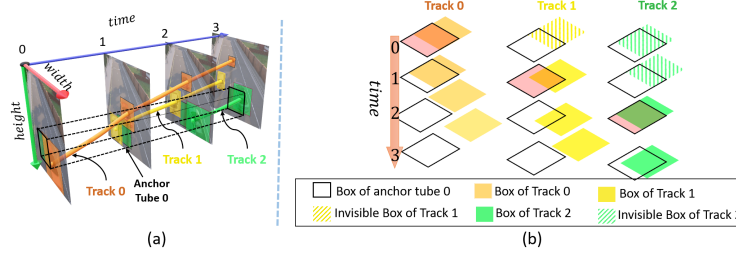


**Fig. 3.** (a) One anchor tube and three tracks are shown to illustrate the search for the best track of the anchor tube. (b) is the simplified demonstration of (a). Based on the largest overlap between the first tube box and the first *visible* track box, Track 2 is selected as the best match.

boxes to 0. We also remove the tracks whose ratio of fully occluded boxes are greater than  $\delta_v$ . We let  $N_F = 16$  in our experiments.

## 4.2 Anchor Tubes

Inspired by the effective Single Shot Detector (SSD) [26] for object detection, we extend the core concept of this technique for MOT. Analogous to the anchor boxes of SSD, we introduce *anchor tubes* for DMM-Net. Here, an anchor tube is a set of anchor boxes (and associated object class and visibility), that share the same location in multiple frames along the temporal dimension (see supplementary material for further visualization). The information of anchor tubes is encoded with the tensors  $\mathbf{B}_{t_1:t_2}$ ,  $\mathbf{C}_{t_1:t_2}$ , and  $\mathbf{V}_{t_1:t_2}$ . The DMM-Net is designed to predict the tube shape offset parameters along the temporal dimension, the confidence for each object class, and the visibility of each box in the tube.

Computing anchor tubes for network training can also be interpreted as further data preparation for DMM-Net. We first employ a search strategy to find the best-matched track for each anchor tube, and subsequently encode the tubes by their best-matched tracks. For the former, we specify the overlap between an anchor tube and a track as the overlap ratio between the first visible box of the track and the corresponding box in the anchor tube. A simplified illustration of this concept is presented in Fig. 3 with one anchor tube and three tracks. The anchor tube 0 iterates over all the tracks to find the largest overlap ratio. The first box of Track 1 and the first two boxes of Track 2 are occluded. Therefore, the overlap ratio of the anchor box filled red is used for selecting the best-matched track, i.e. Track 2 for the largest overlap.

To encode the anchor tubes, we employ their best-matched tracks ( $\mathbf{B}_{t_1:t_2}$ ) along with the classes ( $\mathbf{C}_{t_1:t_2}$ ) and visibility ( $\mathbf{V}_{t_1:t_2}$ ). We denote a box of the  $i^{\text{th}}$  anchor tube at the  $t^{\text{th}}$  frame as  $a_{i,t} = (a_{i,t}^{cx}, a_{i,t}^{cy}, a_{i,t}^w, a_{i,t}^h)$ , where the superscripts  $cx$  and  $cy$  indicate the  $(x, y)$  location of the center, and  $w, h$  denote the width and height of the box. We use the same notation in the following text as well.



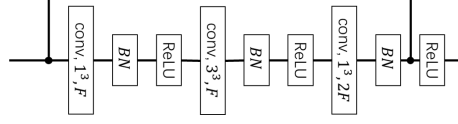


**Fig. 4.** Used ResNeXt block: (conv,  $x^3$ , F) denote ‘F’ convolutional kernels of size  $x \times x \times x$ . BN is Batch Normalization [22] and shortcut connection is summation.

Each anchor box is encoded by the box of its best-matched track as follows:

$$\begin{cases} g_{i,t}^w = \log(b_{i,t}^w/a_{i,t}^w) \\ g_{i,t}^h = \log(b_{i,t}^h/a_{i,t}^h) \\ g_{i,t}^{cx} = (b_{i,t}^{cx} - a_{i,t}^{cx})/a_{i,t}^w \\ g_{i,t}^{cy} = (b_{i,t}^{cy} - a_{i,t}^{cy})/a_{i,t}^h, \end{cases} \quad (1)$$

where  $(b_{i,t}^{cx}, b_{i,t}^{cy}, b_{i,t}^w, b_{i,t}^h)$  describe the box of the best-matched track at the  $t^{\text{th}}$  frame, and  $(g_{i,t}^{cx}, g_{i,t}^{cy}, g_{i,t}^w, g_{i,t}^h)$  represent the resulting encoded box for the best-matched track. Following this encoding, we replace each original box, class, and visibility by its newly encoded counterpart. In the above-mentioned encoding, an anchor tube that has its best-matched track overlap ratio less than  $\delta_o$ , is identified as the ‘background’ class.

### 4.3 Motion Model

For motion modeling, we leverage a quadratic model in time. One of the outputs of DMM-Net is a tensor of motion parameters  $\mathbf{O}_M \in \mathbb{R}^{N_T \times 4 \times N_P}$ , where  $N_P = 3$  in our experiments and  $N_T$  indicates the number of anchor tubes. We estimate an encoded anchor tube for a track as:

$$\begin{cases} \hat{g}_{i,t}^w = p_{11}t^2 + p_{12}t + p_{13} \\ \hat{g}_{i,t}^h = p_{21}t^2 + p_{22}t + p_{23} \\ \hat{g}_{i,t}^{cx} = p_{31}t^2 + p_{32}t + p_{33} \\ \hat{g}_{i,t}^{cy} = p_{41}t^2 + p_{42}t + p_{43}, \end{cases} \quad (2)$$

where  $\hat{g}_{i,t}$  indicates an estimated box descriptor of the  $i^{\text{th}}$  encoded anchor tube at the  $t^{\text{th}}$  frame, the superscripts  $cx$ ,  $cy$ ,  $w$  and  $h$  indicate the center x, center y, height, width of the box respectively, and  $\{p_{11}, \dots, p_{43}\}$  are the motion parameters. Each encoded ground-truth anchor tube can be decoded into a ground truth track by Eq. (1). We further elaborate on the relationship between the motion parameters and the ground truth tracks in the supplementary material. Note that the used motion function is replaceable by any differential function in our technique. We choose quadratic motion modeling considering vehicle tracking as our primary objective.

### 4.4 Architecture

As shown in Fig. 1, our network comprises a Feature Extractor and three sub-network. The network simultaneously processes  $N_F$  video frames for which fea-



**Table 2.** Convolutional groups of the Feature Extractor. Conv is abbreviated as ‘C’, ‘F’ is the number of feature maps, as in Fig. 4, and ‘N’ is the number of bottleneck blocks in each layer.

C1_x	C2_x		C3_x		C4_x		C5_x		C6_x		C7_x	
conv, $7^3$ , 64	F	N	F	N	F	N	F	N	F	N	F	N
	64	3	128	4	256	23	512	3	32	3	32	3

tures are first extracted. The feature maps of six intermediate layers of the Feature Extractor are fed to the sub-networks. These networks predict tensors containing motion parameters ( $\mathbf{O}_M \in \mathbb{R}^{N_T \times N_P \times 4}$ ), object classes ( $\mathbf{O}_C \in \mathbb{R}^{N_T \times N_C}$ ), and visibility information ( $\mathbf{O}_V \in \mathbb{R}^{N_F \times N_T \times 2}$ ).

**Feature Extractor:** We construct our Feature Extractor based on the ResNeXt blocks of the 3D ResNet [20]<sup>5</sup>. The architectural details of the blocks are provided in Fig. 4. The blocks accept ‘F’ channel input that allows us to simultaneously model spatio-temporal features in  $N_F$  frames. We enhance the 3D ResNet architecture by removing the *fully-connected* and *softmax* layers of the network and appending two extra convolutional groups denoted as Conv6\_x and Conv7\_x. We perform this enhancement because the additional convolutional layers are still able to encode further higher level spatio-temporal features of the frames. Details on the convolutional groups used by the Feature Extractor are provided in Table 2. Here, Conv1\_x (abbreviated as C1\_x) contains 64 convolutional kernels of size  $7 \times 7 \times 7$ , stride  $1 \times 2 \times 2$ . A  $3 \times 3 \times 3$  max-pooling layer with stride 2 is inserted before Conv2\_x for down sampling. Each convolutional layer is followed by batch normalization [21] and ReLU [31]. Spatio-temporal down-sampling is performed by Conv3\_1, Conv4\_1 and Conv5\_1 with a stride of 2.

**Sub-networks:** The DMM-Net has three sub-networks to compute motion parameters, object classes, and their visibility. These networks use the outputs of Conv2\_x to Conv7\_x groups of the Feature Extractor. Each sub-network processes the input with six convolutional layers. The architectural details of all three sub-networks are summarized in Table 3. The kernel shape, padding size and stride are the same for each network, whereas the employed numbers of kernels are different. We fix the temporal kernel size for each network to  $\{8, 4, 2, 1, 1, 1\}$ . Denoting the numbers of anchor tubes defined for the six input feature maps of a sub-network by  $\mathcal{K}$ , we let  $\mathcal{K} = \{10, 8, 8, 5, 4, 4\}$  in our experiments. For each sub-network, we concatenate the output feature maps of each convolutional layer. We reshape the concatenated feature according to the dimensions mentioned in the last row of the table. These outputs are subsequently used to compute the network loss.

**Network Loss:** Based on the architecture, the overall loss of DMM-Net is defined as a weighted sum of three sub-losses, including the motion loss ( $\mathcal{L}_M$ ), the classification loss ( $\mathcal{L}_C$ ) and the visibility loss ( $\mathcal{L}_V$ ), given as:

$$\mathcal{L} = \frac{1}{N}(\alpha\mathcal{L}_M + \beta\mathcal{L}_C + \mathcal{L}_V), \quad (3)$$

<sup>5</sup> Notation are adopted from the original work.

**Table 3.** Details of the Motion Subnet (M.S.), Classifier Subnet (C.S.), and Visibility Subnet (V.S.): K.S., P.S., S.S., and N.K. respectively denote the kernel shape, padding size, stride size, and the number of kernels. The row ‘Output’ reports output tensor shape.  $\mathcal{K} = \{10, 8, 8, 5, 4, 4\}$  is the number of anchor tubes for each of the six input feature maps for each sub-network.

	M.S.	C.S.	V.S.
K.S.	$\{8, 4, 2, 1, 1, 1\} \times 3 \times 3$		
P.S.	$0 \times 1 \times 1$		
S.S.	$1 \times 1 \times 1$		
N.K.	$4\mathcal{K}N_P$	$\mathcal{K}N_C$	$2\mathcal{K}$
Output	$N_T \times N_P \times 4$	$N_T \times N_C$	$N_F \times N_T \times 2$

where  $N$  is the number of *positive* anchor tubes, and  $\alpha, \beta$  are both hyper-parameters. The positive anchor tubes exclude the background tubes.

The motion loss  $\mathcal{L}_M$  is defined as the sum of *Smooth*-L1 losses between the ground truth encoded tracks  $g_{i,t}$  and their predicted encoded tracks  $\hat{g}_{i,t}$ , formally:

$$\mathcal{L}_M = \sum_{t=0}^{N_F-1} \sum_{i \in Pos} \sum_{m \in \{cx, cy, h, w\}} \|g_{i,t}^m - \hat{g}_{i,t}^m\|_1, \quad (4)$$

where  $Pos$  is the set of positive encoded anchor tube indices. We compute  $\hat{g}_{i,t}^m$  using Eq. (2) discussed in Section 4.3.

For the classification loss  $\mathcal{L}_C$ , we employ the hard negative mining strategy [26] to balance the positive and negative anchor tubes, where the negative tubes correspond to the background. We denote  $x_{i,j,t}^p \in \{1, 0\}$  to be an indicator for matching the  $i^{\text{th}}$  anchor tube and the  $j^{\text{th}}$  ground-truth track of class ‘ $p$ ’ at the  $t^{\text{th}}$  frame. Each anchor tube at least has one best-matched ground-truth track, implying  $\sum_i x_{i,j,t}^p \geq 1$  for any  $t$ . The classification loss of the DMM-Net is defined as:

$$\mathcal{L}_C = \sum_{t=0}^{N_F} \left( - \sum_{i \in Pos} x_{i,j,t}^p \log(\hat{c}_{i,t}^p) - \sum_{i \in Neg} \log(\hat{c}_{i,t}^0) \right), \quad (5)$$

where  $\hat{c}_{i,t}^p = \frac{\exp c_{i,t}^p}{\sum_p \exp c_{i,t}^p}$  such that  $c_{i,t}^p$  is the predicted confidence of the object being for class  $p : p \in \{1, \dots, N_C\}$ ,  $Neg$  is the set of negative encoded anchor tube indices. We also consider the visibility estimation task fro classification viewpoint and classify each positive box into invisible ‘0’ or visible ‘1’ box. Based on that, the loss is computed as:

$$\mathcal{L}_V = \sum_{t=0}^{N_F} \left( - \sum_{i \in Pos} y_{i,j,t}^q \log(\hat{v}_{i,t}^q) \right), \quad (6)$$

where  $\hat{v}_{i,t}^q = \frac{\exp v_{i,t}^q}{\sum_q \exp v_{i,t}^q}$ , and  $y_{i,j,t}^q$  is an indicator for matching the  $i^{\text{th}}$  anchor tube and the  $j^{\text{th}}$  ground-truth track of visibility ‘ $q$ ’ at the  $t^{\text{th}}$  frame, such that  $q \in \{0, 1\}$ .

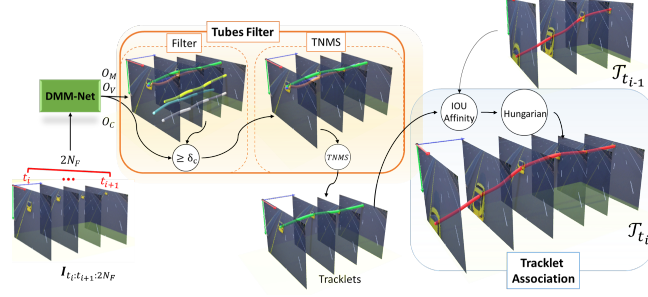


**Fig. 5.** Deployment of DMM-Net: For the  $2N_F$  frames  $I_{t_i:t_{i+1}:2N_F}$  from  $t_i$  to  $t_{i+1}$ , the trained DMM-Net selects  $N_F$  frames as its input and outputs predicted tubes encoded by object motion parameter matrix ( $O_M$ ), classification matrix ( $O_C$ ) and visibility matrix ( $O_V$ ). These matrices are filtered and the track set  $\mathcal{T}_{t_i}$  is updated by associating the filtered tracklets by their IOU with the previous track set  $\mathcal{T}_{t_{i-1}}$ .

#### 4.5 Deployment

The trained DMM-Net is readily deployable for tracking (Fig. 5). The overall tracker processes  $2N_F$  frames  $I_{t_i:t_{i+1}:2N_F}$ , where the DMM-Net first selects  $N_F$  consecutive frames and outputs the predicted tubes encoded with object motion parameters, classes and visibility using Eq. (2). The tubes are decoded with Eq. (1). A filtration is then done to remove the undesired tubes and we get tracklets (details to follow). We compute updated trajectory set  $\mathcal{T}_{t_i}$  by associating the tracklets with the previous trajectory set  $\mathcal{T}_{t_{i-1}}$  using their IOUs.

To filter, we first remove tubes with confidence lower than a threshold  $\delta_c$ . We subsequently perform a Tube None Maximum Suppression (TNMS). To that end, we cluster the detected tubes of the same category into multiple groups by their IOUs with a threshold  $\delta_{nms}$ . Then, we only keep one tube for each group that has the maximum confidence of being positive. The kept tubes, namely “tracklets”, are employed to update trajectory set.

We initialize our track set  $\mathcal{T}_{t_i}$  with as many trajectories as the number of tracklets. The track set is updated from  $t_i^{\text{th}}$  to  $t_{i+1}^{\text{th}}$  stamp using the Hungarian algorithm [30] applied to an IOU matrix  $\Psi \in \mathbb{R}^{n'_{t_{i-1}} \times n_{t_i}}$ , where  $n'_{t_{i-1}}$  is the number of element in the previous track set, and  $n_{t_i}$  is the number of tracklets. Notice that we perform association of tracklets and not the individual objects. The object association remains implicit and is done inside the DMM-Net which lets us define the tubes. The association of tracklets, defined across multiple frames, leads to significant computational gain. This is one of the core reasons of the orders of magnitude gain in the tracking speed of our technique over existing methods, as will be clear in Section 5.

To form the matrix  $\Psi$ , we must compute IOU between the existing tracklets and the new tracklets. Fig. 6 shows the procedure adopted for calculating the IOU between two tracklets with a simplified example. Overall, our tracker is an on-line technique in the sense that it does not use future frames to predict

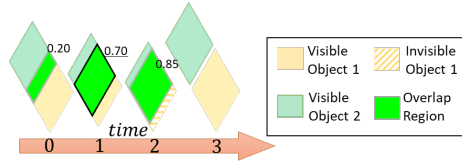


**Fig. 6.** Example of calculating Tube IOU. There are two tracklets (yellow, cyan). Their intersection is green. The tracklet IOU is the maximum IOU of the visible box pair. Although IOU at  $t = 2$  is the largest, the lined yellow object is invisible, hence, we select the second largest IOU at  $t = 1$  as the tracklet IOU.

object trajectories. Concurrently, DMM-Net can perform tracking in real-time that makes it a highly desirable technique for practical applications.

## 5 Experiments

We evaluate our technique using the proposed Omni-MOT dataset and the popular UA-DETRAC challenge [45]. The former is to demonstrate both the effectiveness of our network for MOT and trainability of deep models for MOT with Omni-MOT. We mainly focus on ‘vehicle’ tracking in this work. The proposed dataset is also for the vehicle tracking problem. Whereas DMM-Net is trained here for vehicle tracking, it is possible to train it for e.g. pedestrian tracking.

**Implementation Details:** We implement the DMM-Net using Pytorch [32] and train it using NVIDIA GeForce GTX Titan GPU. The hyper-parameter values are selected with cross-validation to maximize the MOTA metric on the validation set of UA-DETRAC. The chosen values of the hyperparameters are as follows. Batch size  $B = 8$ , number of training epochs per model = 20, number of input frames = 16, input frame size =  $168 \times 168$ , We use Adam Optimizer [24] for training. Other hyper-parameter values are  $\delta_c = 0.4$ ,  $\delta_{nms} = 0.3$ , and  $\delta_o = 0.5$ .

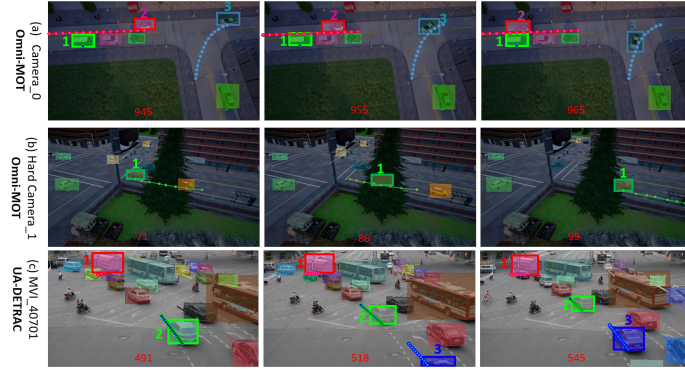
**Omni-MOT dataset:** To demonstrated the efficacy of DMM-Net and trainability of deep models on our dataset, we select five scenes from the Omni-MOT and perform tracking. The scenes are chosen with Easy camera viewpoint with clear weather conditions. The selected scenes are from Town 02 (with 50 vehicles) that are indexed 0, 1, 5, 7 and 8 in the dataset. In this experiment, we train and test DMM-Net using the train and test partitions of the selected scene, as provided by Omni-MOT. Our training required 59.2 hours for 22 epochs.

We use both CLEAR MOT [5], and MT/ML [35] metrics and summarize the results in Table 4. For the definitions of metrics we refer to the original works. We refer to [25] for the details on the comprehensive metrics MOTA and MOTAP. The table provides metric values for both training and test partitions. The variation between these values is a clear indication that despite the Easy camera view, the dataset provides reasonable challenges for the MOT task. We provide results with additional view points in the supplementary material to further put the reported values into better perspective.

An illustration of tracking for Camera\_0 is also provided in Fig. 7 (top). Our technique is able to easily track vehicles that are stationary, (e.g. 1), moving

**Table 4.** Results on Omni-MOT: The symbol  $\uparrow$  indicates higher values are better, and  $\downarrow$  implies lower values are favored.

Type	Camera	IDF1 $\uparrow$	IDP $\uparrow$	IDR $\uparrow$	Rcll $\uparrow$	Prcn $\uparrow$	GT $\uparrow$	MT $\uparrow$	PT $\uparrow$	ML $\downarrow$	FP $\downarrow$	FN $\downarrow$	IDs $\downarrow$	FM $\downarrow$	MOTA $\uparrow$	MOTP $\uparrow$
Test	Camera_0	72.2%	69.3%	75.4%	90.6%	83.2%	41	38	3	0	1762	911	18	98	72.1%	79.3%
	Camera_1	59.3%	56.2%	62.7%	81.9%	73.4%	35	19	15	1	1199	730	12	61	52.0%	75.5%
	Camera_5	40.2%	61.3%	29.9%	34.7%	71.1%	44	9	20	15	2779	12855	38	80	20.4%	76.1%
	Camera_7	77.8%	79.6%	76.1%	88.3%	92.4%	37	29	8	0	1518	2457	20	99	80.9%	80.3%
	Camera_8	30.5%	47.3%	22.5%	33.5%	70.7%	38	0	28	10	1789	8548	36	110	19.3%	70.3%
Train	Camera_0	59.2%	58.6%	59.7%	87.7%	86.0%	48	40	8	0	2517	2174	43	172	73.2%	79.5%
	Camera_1	47.6%	44.2%	51.6%	80.0%	68.6%	46	29	16	1	3681	2005	50	137	42.9%	76.9%
	Camera_5	45.0%	52.7%	39.2%	57.0%	76.7%	49	6	37	6	4844	12000	122	234	39.2%	77.3%
	Camera_7	74.7%	71.9%	77.8%	90.1%	83.3%	43	31	12	0	1804	985	16	91	71.8%	79.7%
	Camera_8	41.7%	52.2%	34.7%	44.1%	66.3%	43	0	41	2	1884	4705	18	117	21.4%	68.3%
Average		55.5%	61.1%	50.9%	66.5%	79.8%	424	201	188	35	23777	47370	373	1199	49.4%	77.8%

**Fig. 7.** Tracking illustration of DMM-Net on Omni-MOT (first and second row) and UA-DETRAC (third row). The mentioned IDs are for reference in the text only.

along a straight path (e.g. 2), and moving along a curved path (e.g. 3), which justifies the selection of our motion model. Additionally, our tracker has the power to deal with even full occlusions between the frames. We show such a case for a hard camera view point in the middle row of Fig. 7. In this case, vehicle-1 is totally occluded at the 86<sup>th</sup> frame which can be detected and tracked by our tracker. At the 99<sup>th</sup> frame, vehicle-1 is partially occluded, but the track-lets association performs correctly. Note that, our tracker does not need to be evaluated with (detector-based) UA-DETRAC metrics [45] as the Omni-MOT dataset provides ground truth detections without using off-the-shelf detectors.

**UA-DETRAC:** The UA-DETRAC challenge [45] is arguably the most widely used large-scale benchmark for MOT of vehicles. It comprises 100 videos @ 25 fps, recorded in 24 locations with frame size  $540 \times 960$ . For this challenge, results are computed by a remote server using CLEAR MOT and MT/ML metrics with Precision-Recall curve of the detection. We refer to [45] for further details on the metrics. In Table 5, we show our results on the UA-DETRAC challenge. The pre-fix PR for the metrics indicates the use of Precision-Recall curve. It can be seen that DMM-Net achieves excellent MOTA score, which is widely considered as the most comprehensive metric for MOT. We also provide results for DMM-Net+ which augments the UA-DETRAC training set with a subset of

**Table 5.** Results on UA-DETRAC: ‘T.S.’ is tracker speed (fps), ‘D.S.’ is detector speed (fps), and ‘A.S.’ is the overall speed (fps). The DMM-Net does not need explicit detector. DMM-Net+ uses a subset of Omni-MOT for data augmentation.

Tracker	Detector	PR-MOTA $\uparrow$	PR-MT $\uparrow$	PR-ML $\downarrow$	PR-IDS $\downarrow$	PR-FRAG $\downarrow$	PR-FP $\downarrow$	PR-FN $\downarrow$	T.S. $\uparrow$	D.S. $\uparrow$	A.S. $\uparrow$
CEM [1]	ACF [12]	4.50%	2.90%	37.10%	265.4	366.0	15180.3	270643.2	3.74	0.67	0.57
CMOT [49]	ACF [12]	7.80%	14.30%	20.70%	418.3	2161.7	81401.4	183400.2	3.12	0.67	0.55
DCT [2]	ACF [12]	7.90%	4.80%	34.40%	108.1	101.4	13059.7	251166.4	1.29	0.67	0.44
GOG [33]	ACF [12]	10.80%	12.20%	22.30%	3950.8	3987.3	45201.5	197094.2	319.29	0.67	0.67
H2T [47]	ACF [12]	8.20%	13.10%	21.30%	1122.8	1445.8	71567.4	189649.1	1.08	0.67	0.41
IHTLS [11]	ACF [12]	6.60%	11.50%	22.40%	1243.1	4723.0	72757.5	198673.5	5.09	0.67	0.59
CEM [1]	DPM [16]	3.30%	1.30%	37.80%	265	317.1	13888.7	270718.5	4.49	0.17	0.16
DCT [2]	DPM [16]	2.70%	0.50%	42.70%	72.2	<b>68.8</b>	7785.8	280762.2	2.85	0.17	0.16
GOG [33]	DPM [16]	5.50%	4.10%	27.70%	1873.9	1988.5	38957.6	230126.6	476.52	0.17	0.17
IOU $\uparrow$ [6]	DPM [16]	1.92%	0.84%	43.70%	<b>61.4</b>	106.0	<b>3111.5</b>	290412.2	100842	0.17	0.17
CEM [1]	R-CNN [19]	2.70%	2.30%	34.10%	778.9	1080.4	34768.9	269043.8	5.4	0.1	0.10
DCT [2]	R-CNN [19]	11.70%	10.10%	22.80%	758.7	742.9	336561.2	210855.6	0.71	0.1	0.09
CMOT [49]	R-CNN [19]	11.00%	<b>15.70%</b>	19.00%	506.2	22551.1	74253.6	<b>177532.6</b>	3.59	0.1	0.10
GOG [33]	R-CNN [19]	10.00%	13.50%	20.10%	7834.5	7401.0	58378.5	192302.7	352.8	0.1	0.10
H2T [47]	R-CNN [19]	11.10%	14.60%	19.80%	1481.9	1820.8	66137.2	184358.2	2.78	0.1	0.10
IHTLS [11]	R-CNN [19]	8.30%	12.00%	21.40%	1536.4	5954.9	68662.6	199268.8	11.96	0.1	0.10
DMM-Net	-	<b>11.80%</b>	10.30%	<b>15.20%</b>	230.3	658.0	36238.8	194886.4	-	-	<b>123.25</b>
DMM-Net+	-	<b>12.20%</b>	10.80%	<b>14.90%</b>	228.2	674.1	36355.8	192289.6	-	-	<b>123.25</b>

Omni-MOT. This subset contained 8 random videos from Omni-MOT. We can see an overall performance gain with this augmentation, exemplifying the utility of Omni-MOT in data augmentation.

Notice that our technique does not require an external ‘detector’ and achieves highly promising PR-MOTA score for UA-DETRAC @ 120+ fps - orders of magnitude faster than the existing methods. In the third row of Fig. 7, we show an example of tracking result. The box color indicates the predicted object identity. Our tracker leverages information from previous frames to detect partially occluded objects, e.g. vehicle-3 in frame 518. The figure also shows the generalization power of our in-built detection mechanism. For instance, vehicle-1 is a very rare vehicle that is consistently assigned the correct identity. In the supplementary material, we provide further example tracking videos that clearly demonstrate successful tracking by DMM-Net for UA-DETRAC.

## 6 Conclusion

In the context of tracking-by-detection, we proposed a deep network DMM-Net that removes the need for an explicit external detector and performs tracking at 120+ fps to achieve 12.80% PR-MOTA value on the UA-DETRAC challenge. Our network meticulously models object motions, classes and their visibility that are subsequently used for efficiently associating the object tracks. The proposed network provides an end-to-end solution for detection and tracklet generation across multiple video frames. We also propose a realistic CARLA simulator based large-scale dataset with over 14M frames for vehicle tracking. The dataset provides precise and comprehensive ground truth with full control over data parameters, which allows for the much needed transparency in evaluation. We also provide scripts to generate more data under our framework and we make the code of DMM-Net public.

## References

1. Andriyenko, A., Schindler, K.: Multi-target tracking by continuous energy minimization. In: Proceedings of the IEEE Computer Society Conference on Computer Vision and Pattern Recognition. pp. 1265–1272 (2011). <https://doi.org/10.1109/CVPR.2011.5995311> 14
2. Andriyenko, A., Schindler, K., Roth, S.: Discrete-continuous optimization for multi-target tracking. In: Proceedings of the IEEE Computer Society Conference on Computer Vision and Pattern Recognition. pp. 1926–1933 (2012). <https://doi.org/10.1109/CVPR.2012.6247893> 14
3. Bae, S.H., Yoon, K.J.: Confidence-Based Data Association and Discriminative Deep Appearance Learning for Robust Online Multi-Object Tracking. *IEEE Transactions on Pattern Analysis and Machine Intelligence* **40**(3), 595–610 (2018). <https://doi.org/10.1109/TPAMI.2017.2691769> 4
4. Berclaz, J., Fleuret, F., Türetken, E., Fua, P.: Multiple object tracking using k-shortest paths optimization. *IEEE TPAMI* **33**(9), 1806–1819 (2011). <https://doi.org/10.1109/TPAMI.2011.21> 3
5. Bernardin, K., Stiefelhagen, R.: Evaluating multiple object tracking performance: The CLEAR MOT metrics. *Eurasip Journal on Image and Video Processing* **2008** (2008). <https://doi.org/10.1155/2008/246309> 12
6. Bochinski, E., Eiselein, V., Sikora, T.: High-Speed tracking-by-detection without using image information. 2017 14th IEEE International Conference on Advanced Video and Signal Based Surveillance, AVSS 2017 (2017). <https://doi.org/10.1109/AVSS.2017.8078516> 14
7. Butt, A.A., Collins, R.T.: Multi-target tracking by lagrangian relaxation to min-cost network flow. In: Proc. CVPR. pp. 1846–1853 (2013) 3
8. Chari, V., Lacoste-Julien, S., Laptev, I., Sivic, J.: On pairwise costs for network flow multi-object tracking. *Proc. CVPR* **07-12-June**, 5537–5545 (2015). <https://doi.org/10.1109/CVPR.2015.7299193> 3
9. Dai, J., Li, Y., He, K., Sun, J.: R-fcn: object detection via region-based fully convolutional networks. In: NIPS’16 Proceedings of the 30th International Conference on Neural Information Processing Systems. pp. 379–387 (2016), <https://academic.microsoft.com/paper/2407521645> 4
10. Dehghan, A., Modiri Assari, S., Shah, M.: Gmmcp tracker: Globally optimal generalized maximum multi clique problem for multiple object tracking. In: Proc. CVPR. pp. 4091–4099 (2015) 1, 3
11. Dicle, C., Camps, O.I., Sznai, M.: The way they move: Tracking multiple targets with similar appearance. In: Proceedings of the IEEE International Conference on Computer Vision. pp. 2304–2311 (2013). <https://doi.org/10.1109/ICCV.2013.28614>
12. Dollar, P., Appel, R., Belongie, S., Perona, P.: Fast feature pyramids for object detection. *IEEE Transactions on Pattern Analysis and Machine Intelligence* (2014). <https://doi.org/10.1109/TPAMI.2014.2300479> 14
13. Dosovitskiy, A., Ros, G., Codevilla, F., Lopez, A., Koltun, V.: CARLA: An Open Urban Driving Simulator. In: Proceedings of the 1st Annual Conference on Robot Learning. pp. 1–16 (2017), <http://arxiv.org/abs/1711.03938> 3, 4
14. Emami, P., Pardalos, P.M., Eleftheriadou, L., Ranka, S.: Machine Learning Methods for Solving Assignment Problems in Multi-Target Tracking. *arXiv:1802.06897* **1**(1), 1–35 (2018) 3



15. Feichtenhofer, C., Pinz, A., Zisserman, A.: Detect to Track and Track to Detect. Proceedings of the IEEE International Conference on Computer Vision **2017-Octob**, 3057–3065 (2017). <https://doi.org/10.1109/ICCV.2017.330> 4
16. Felzenszwalb, P.F., Girshick, R.B., McAllester, D., Ramanan, D.: Object detection with discriminatively trained part-based models. IEEE TPAMI **32**(9), 1627–1645 (2010) 14
17. Ferryman, J., Shahrokni, A.: PETS2009: Dataset and challenge. In: Proceedings of the 12th IEEE International Workshop on Performance Evaluation of Tracking and Surveillance, PETS-Winter 2009 (2009). <https://doi.org/10.1109/PETS-WINTER.2009.5399556> 4
18. Geiger, A., Lenz, P., Urtasun, R.: Are we ready for autonomous driving? the KITTI vision benchmark suite. In: Proceedings of the IEEE Computer Society Conference on Computer Vision and Pattern Recognition. pp. 3354–3361 (2012). <https://doi.org/10.1109/CVPR.2012.6248074> 4
19. Girshick, R., Donahue, J., Darrell, T., Malik, J.: Rich feature hierarchies for accurate object detection and semantic segmentation. In: Proceedings of the IEEE Computer Society Conference on Computer Vision and Pattern Recognition (2014). <https://doi.org/10.1109/CVPR.2014.81> 14
20. Hara, K., Kataoka, H., Satoh, Y.: Can Spatiotemporal 3D CNNs Retrace the History of 2D CNNs and ImageNet? CVPR pp. 6546–6555 (2018). <https://doi.org/10.1109/CVPR.2018.00685>, <http://arxiv.org/abs/1711.09577> 2, 9
21. He, K., Zhang, X., Ren, S., Sun, J.: Deep residual learning for image recognition. In: Proceedings of the IEEE Computer Society Conference on Computer Vision and Pattern Recognition (2016). <https://doi.org/10.1109/CVPR.2016.90> 9
22. Ioffe, S., Szegedy, C.: Batch normalization: Accelerating deep network training by reducing internal covariate shift. arXiv (2015) 8
23. Iqbal, U., Milan, A., Gall, J.: PoseTrack: Joint multi-person pose estimation and tracking. In: Proceedings - 30th IEEE Conference on Computer Vision and Pattern Recognition, CVPR 2017 (2017). <https://doi.org/10.1109/CVPR.2017.495> 4
24. Kingma, D.P., Ba, J.L.: Adam: A Method for Stochastic Optimization. In: ICLR 2015 : International Conference on Learning Representations 2015 (2015), <https://academic.microsoft.com/paper/2964121744> 12
25. Leal-Taixé, L., Milan, A., Reid, I., Roth, S., Schindler, K.: MOTChallenge 2015: Towards a Benchmark for Multi-Target Tracking. arXiv:1504.01942 [cs] pp. 1–15 (2015), <http://arxiv.org/abs/1504.01942> 1, 4, 12
26. Liu, W., Anguelov, D., Erhan, D., Szegedy, C., Reed, S., Fu, C.Y., Berg, A.C.: SSD: Single shot multibox detector. ECCV **9905 LNCS**, 21–37 (2016). [https://doi.org/10.1007/978-3-319-46448-0\\_2](https://doi.org/10.1007/978-3-319-46448-0_2) 3, 7, 10
27. Luo, W., Xing, J., Milan, A., Zhang, X., Liu, W., Zhao, X., Kim, T.K.: Multiple Object Tracking: A Literature Review. arXiv:1409.7618v4 pp. 1–18 (2017). <https://doi.org/10.1145/0000000.0000000> 1, 3
28. Milan, A., Leal-Taixé, L., Reid, I., Roth, S., Schindler, K.: MOT16: A Benchmark for Multi-Object Tracking. CoRR **abs/1603.0** (2016), <http://arxiv.org/abs/1603.00831> 4
29. Milan, A., Roth, S., Schindler, K.: Continuous energy minimization for multitarget tracking. IEEE Transactions on Pattern Analysis and Machine Intelligence **36**(1), 58–72 (2014). <https://doi.org/10.1109/TPAMI.2013.103> 4
30. Munkres, J.: Algorithms for the Assignment and Transportation Problems. Journal of the Society for Industrial and Applied Mathematics **5**(1), 32–38 (1957). <https://doi.org/10.1137/0105003> 11

31. Nair, V., Hinton, G.: Rectified Linear Units Improve Restricted Boltzmann Machines. In: Proceedings of the 27th International Conference on Machine Learning (2010) [9](#)
32. Paszke, A., Chanan, G., Lin, Z., Gross, S., Yang, E., Antiga, L., Devito, Z.: Automatic differentiation in PyTorch. *Advances in Neural Information Processing Systems* 30 (Nips), 1–4 (2017) [12](#)
33. Pirsiavash, H., Ramanan, D., Fowlkes, C.C.: Globally-optimal greedy algorithms for tracking a variable number of objects. *Proceedings of the IEEE Computer Society Conference on Computer Vision and Pattern Recognition* pp. 1201–1208 (2011). <https://doi.org/10.1109/CVPR.2011.5995604> [3](#), [14](#)
34. Reid, D., et al.: An algorithm for tracking multiple targets. *IEEE transactions on Automatic Control* **24**(6), 843–854 (1979) [3](#)
35. Ristani, E., Solera, F., Zou, R., Cucchiara, R., Tomasi, C.: Performance measures and a data set for multi-target, multi-camera tracking. In: *Lecture Notes in Computer Science (including subseries Lecture Notes in Artificial Intelligence and Lecture Notes in Bioinformatics)*. vol. 9914 LNCS, pp. 17–35 (2016). [https://doi.org/10.1007/978-3-319-48881-3\\_2](https://doi.org/10.1007/978-3-319-48881-3_2) [12](#)
36. Ristani, E., Tomasi, C.: Tracking Multiple People Online and in Real Time. In: *Asian Conference on Computer Vision*. pp. 444–459. Springer (2014) [4](#)
37. Roshan Zamir, A., Dehghan, A., Shah, M.: GMCP-tracker: Global multi-object tracking using generalized minimum clique graphs. In: *Lecture Notes in Computer Science* (2012). [https://doi.org/10.1007/978-3-642-33709-3\\_25](https://doi.org/10.1007/978-3-642-33709-3_25) [3](#)
38. Shafique, K., Shah, M.: A noniterative greedy algorithm for multiframe point correspondence. *IEEE transactions on pattern analysis and machine intelligence* **27**(1), 51–65 (2005) [3](#)
39. Sheng, H., Zhang, Y., Chen, J., Xiong, Z., Zhang, J.: Heterogeneous association graph fusion for target association in multiple object tracking. *IEEE Transactions on Circuits and Systems for Video Technology* (2018) [3](#)
40. Shitrit, H.B., Berclaz, J., Fleuret, F., Fua, P.: Multi-commodity network flow for tracking multiple people. *IEEE TPAMI* **36**(8), 1614–1627 (2014) [3](#)
41. Shu, G., Dehghan, A., Oreifej, O., Hand, E., Shah, M.: Part-based multiple-person tracking with partial occlusion handling. In: *Proc. CVPR*. pp. 1815–1821. IEEE (2012) [3](#)
42. Sun, S., Akhtar, N., Song, H., Mian, A., Shah, M.: Deep Affinity Network for Multiple Object Tracking **13**(9), 1–15 (2018), <http://arxiv.org/abs/1810.11780> [1](#), [4](#), [6](#)
43. Tian, Y., Dehghan, A., Shah, M.: On detection, data association and segmentation for multi-target tracking. *IEEE Transactions on Pattern Analysis and Machine Intelligence* pp. 1–1 (2018) [1](#), [3](#)
44. Voigtlaender, P., Krause, M., Osep, A., Luiten, J., Sekar, B.B.G., Geiger, A., Leibe, B.: Mots: Multi-object tracking and segmentation. In: *Proc. CVPR*. pp. 7942–7951 (2019) [1](#)
45. Wen, L., Du, D., Cai, Z., Lei, Z., Chang, M.C., Qi, H., Lim, J., Yang, M.H., Lyu, S.: UA-DETRAC: A New Benchmark and Protocol for Multi-Object Detection and Tracking (2015), <http://arxiv.org/abs/1511.04136> [3](#), [4](#), [12](#), [13](#)
46. Wen, L., Du, D., Li, S., Bian, X., Lyu, S.: Learning non-uniform hypergraph for multi-object tracking. In: *Proceedings of the AAAI Conference on Artificial Intelligence*. vol. 33, pp. 8981–8988 (2019) [3](#)
47. Wen, L., Li, W., Yan, J., Lei, Z., Yi, D., Li, S.Z.: Multiple target tracking based on undirected hierarchical relation hypergraph. *Proceedings of the IEEE Computer*

- Society Conference on Computer Vision and Pattern Recognition **1**, 1282–1289 (2014). <https://doi.org/10.1109/CVPR.2014.167> **4**, **14**
48. Wu, B., Nevatia, R.: Detection and tracking of multiple, partially occluded humans by bayesian combination of edgelet based part detectors. *International Journal of Computer Vision* **75**(2), 247–266 (2007) **3**
49. Zhu, J., Yang, H., Liu, N., Kim, M.: Online Multi-Object Tracking with Dual Matching Attention Networks pp. 1–17 **14**

# Simultaneous Detection and Tracking with Motion Modelling for Multiple Object Tracking (Supplementary Material)

ShiJie Sun<sup>1</sup>, Naveed Akhtar<sup>2</sup>, XiangYu Song<sup>3</sup>, HuanSheng Song<sup>1</sup>, Ajmal Mian<sup>2</sup>, and  
Mubarak Shah<sup>4</sup>

<sup>1</sup> Chang'an University, Xi'an, Shaanxi, China  
{shijieSun, hshsong}@chd.edu.cn

<sup>2</sup> University of Western Australia, 35 Stirling Highway, Crawley, WA, Australia  
{naveed.akhtar, ajmal.mian}@uwa.edu.au

<sup>3</sup> Deakin University, RWaurm Ponds, Victoria 3216, Melbourne, Australia  
xiangyu.song@deakin.edu.au

<sup>4</sup> University of Central Florida, Orlando, FL, America  
shah@crcv.ucf.edu

## A Public Source Code & Dataset

Along with the submitted manuscript, we provide the source code of the proposed DMM-Net and publish the proposed Omni-MOT dataset. We also provide our implementation to generate more videos similar to the proposed dataset using the CARLA simulator [3]. Below, the links are provided for anonymous repositories for the sake of the review process. The links will be made public after the acceptance. (Click on the highlighted text to open the URL).

- **DMM-Net** is the source code of DMM-Net. It also contains the training and testing script for both UA-DETRAC [10] and Omni-MOT dataset, and instructions for reproducing the result of our methods.
- **Omni-MOT Dataset** provides the link to the dataset along with the related description.
- **Omni-MOT Script** is the source code for generating the Omni-MOT dataset and extending it. It includes the script for recording the MOT data and playing the recorded dataset.

## B Videos for Dataset and Further Results

We provide the following videos for the review process. These and further videos will also be made public after the acceptance:

- **Omni-MOT dataset videos** illustrates different scenes, camera viewpoints and weather conditions used in the generated large-scale realistic dataset.
- **Further results on Omni-MOT** illustrates more tracking results on the proposed dataset.
- **Further results on UA-DETRAC** show tracking results on a representative scene from the UA-DETRAC challenge.

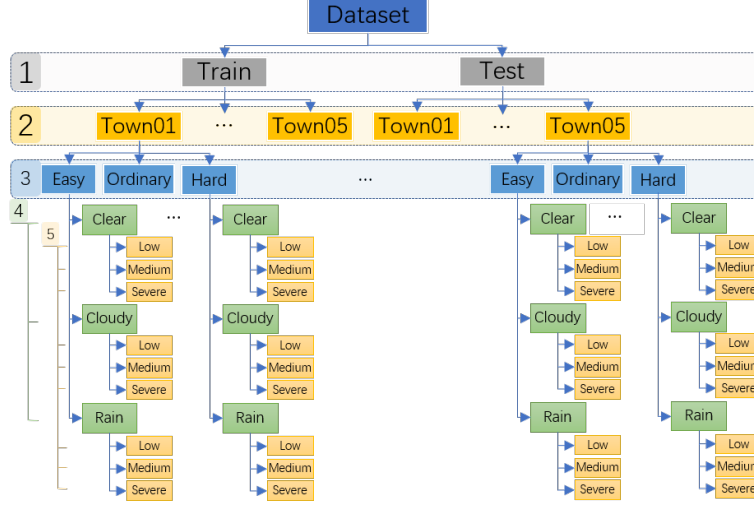


Fig. 1. Overall structure of the Omni-MOT dataset.

## C Further Details of the Dataset

The structure of the proposed dataset can be best understood under five dimensions of divisions. We depict these dimensions as different levels of a block diagram in Fig. 1 for a clear overview. Along the first dimension, we split the dataset into the training and testing sets. Along the second, five towns of the CARLA simulator are employed for making the dataset diverse. For each town, we set the camera with different viewpoints for the third dimension of division. These viewpoints include three levels of difficulty, namely, Easy, Ordinary, and Hard level. Along the fourth dimension, different weather conditions split the data. These weather conditions contain Clear, Cloudy, and Rainy weather. The last variability that makes our data diverse consists of three congestion levels, namely; Low, Medium, and Severe congestion. Details are given below.

**Train/Test split:** The training set consists of 1,755 videos, 8,775K frames, 134.2K tracks, and 68.88M boxes. The testing set includes 1,755 videos, 5,265K frames, 122.37K tracks and 41.36M boxes.

**Towns:** There are five towns in our dataset, whose details are given in Table 1. Among these, Town05 is the largest city that also has three overpass roads. Town02 is the smallest city, whereas Town03 also contains a tube. Town04 is the most populous in terms of T-junctions.

**Camera viewpoints:** 39 cameras are placed in each city with different viewpoints. The camera horizontal field of view is  $90^\circ$ . We refer to the **Omni-MOT dataset videos** to visually observe the viewpoints.

**Weather conditions:** Three kinds of weather are simulated, namely, Clear, Cloudy, and Rainy, by changing the weather parameters of the CARLA simulator. These weather parameters include cloudiness and precipitation, and their values range from 0 to 100.

**Table 1.** Details of five towns. Column “Size” is manually measured and its format is  $Width \times Length$ 

Name	Size (m)	Cross	T-junction	Roundabout	Overpass	Tunnel
Town01	$342 \times 413$	0	12	0	0	0
Town02	$205 \times 208$	0	9	0	0	0
Town03	$438 \times 483$	5	14	2	0	1
Town04	$816 \times 914$	8	21	3	1	0
Town05	$430 \times 486$	13	8	0	3	0

**Table 2.** The number of vehicles for each congestion level of different towns.

City	Low	Medium	Severe
Town01	50	75	95
Town02	50	75	95
Town03	100	170	230
Town04	100	170	230
Town05	100	170	230

The cloudiness of Clear is 15, and the cloudiness of Cloudy and Rainy are 80. Both the precipitation of Clear and Cloudy are 0, and the precipitation of Rainy is 60.

**Road congestion:** We include three levels of traffic congestion, i.e. low, medium, and severe congestion. Because cities have different sizes, these congestion levels are decided by different numbers of vehicles. Table 2 summarizes the number of vehicles for the chosen level of congestion in all five towns.

In the proposed dataset, five different simulated cities are considered. For each city, we use up to 39 cameras. The cameras are placed with viewpoints that have three levels of difficulty for the MOT scenarios. Namely, (a) Easy view: which results in no occlusion of the vehicles. (b) Ordinary view: that allows temporary occlusions but forbids continuous occlusions. (c) Hard view: that allows continuous occlusions in the videos. Collectively, we provide 90 scenes in the dataset that result in 3,510 videos. There are 14.04M frames of size  $1920 \times 1080$  in the OMOT dataset that are recorded in the ‘XDIV’ format to provide high-quality videos with acceptable memory size.

### C.1 Comparison to the existing MOT datasets

To put the proposed dataset into a better perspective, we also compare it to the existing popular datasets for the MOT task. In Table 3, we provide the comparison. Our dataset comprises 3,510 videos, 14M+ frames, 250K tracks, and 110M+ bounding boxes, whose frame number is almost 1,200 times larger than MOT17. The number of provided tracks and boxes are 210 and 30 times larger than UA-DETRAC. Besides, for the proposed Omni-MOT, all the boxes and tracks are automatically generated by the enumerator that avoids any labeling error. In the table, we include nuScenes [2] and Waymo [9] for the sake of comprehensive benchmarking. Nevertheless, these datasets are related to self-driving vehicles that are captured with moving cameras.

**Table 3.** Comparison with other popular MOT datasets. Columns “Frames” is the number of frames ( $1k = 10^3, 1M = 10^6$ ), “Tracks” is the number of tracks and “Boxes” is the number of bounding boxes. “-” indicates that no information is provided.

Dataset	Training			Testing		
	Frames	Tracks	Boxes	Frames	Tracks	Boxes
PETS [4]	-	-	-	1.5k	106	18.5k
KITTI [5]	8k	-	-	11k	-	-
TUD [1]	610	-	610	451	31	2.6k
MOT15 [6]	5.5k	500	39.9k	5.8k	721	61k
MOT17 [8]	5.3k	467	110k	5.9k	742	182k
UA-DETRAC [10]	84k	5.9k	578k	56k	2.3k	632k
nuScenes [2]	40k	-	1.4M	-	-	-
Waymo [9]	154k	-	8.6M	23k	-	1.3M
Omni-MOT(Ours)	<b>8775k</b>	<b>134.2k</b>	<b>68.88M</b>	<b>5265k</b>	<b>122.37k</b>	<b>41.36M</b>

**Table 4.** Data format of the ground truth file provided with the dataset.

Index	Name	Description
0	frame index	0-based frame index
1	vehicle id	Unique ID of vehicle (0-based)
2	bbox	Represents left, top, right, and bottom of the vehicle bounding box
6	3d bbox	The 8 points of the vehicles 3D bounding boxes in image coordinates
14	vehicle position	Vehicles center in the world coordinates
17	integrity	Integrity of the vehicle. Binary value in (0, 1)
18	velocity vector	Velocity vector in the world coordinates
21	acceleration vector	Acceleration vector in the world coordinates
24	wheel number	Number of vehicle wheels
25	camera view size	The width and the height of the camera view
27	camera FOV	The field of view of the camera
28	camera position	Camera position in the world coordinates
31	camera rotation	Camera rotation in the world coordinates
34	weather condition	Weather condition in the current frame.

## C.2 On the ground-truth annotations

The ground-truth annotations is generated by the CARLA simulator, which allows us to capture comprehensive information on the target objects with high precision. Hence, besides being accurate, our ground truth annotations are detailed enough to be used for other related problems, such as 3D estimation, velocity estimation, camera calibration, etc. To this end, we bring as much information as we can into the ground truth file. Table 4 gives details of the format of the ground truth files (available through the dataset download link provided above). The “3D bbox” at columns 6-13 contains values describing point coordinates. These points are the image projection of a minimum 3D cuboid envelope of the vehicle in the world coordinates. The column “bbox” is calculated by the minimum rectangle envelope of these points. On index 17, “integrity” encodes the visibility of vehicles. A clear description of the remaining entities is provided in the table.



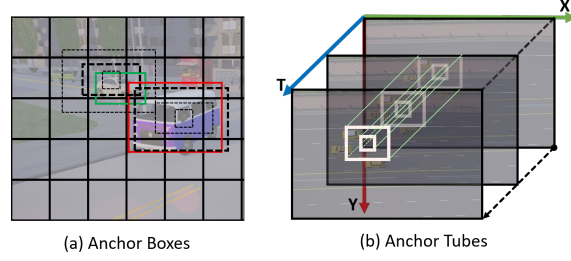


**Fig. 2.** Illustration of the anchor tubes. The anchor boxes in (a) are a set of boxes in the 2D coordinates. The SSD model predicts the scaling and translation parameters relative to each anchor box. Extended from anchor boxes, the anchor tubes in (b) are a set of cuboids in the 3D coordinate. Each anchor tube consists of  $N_F$  boxes. Our proposed network predicts the tube shape offset parameters along the temporal dimension, the confidence for each object class, and the visibility of each box in the tube.

## D Anchor Tubes

The proposed notion of anchor tube is an extension of the concept of anchor boxes in SSD [7]. In our technique, the anchor tubes are pre-defined and distributed at every position of the selected feature maps. An anchor tube is essentially a set of anchor boxes that share the same location in multiple frames along the temporal dimension, as illustrated in Fig. 2. The Fig. 2(a) depicts three pre-defined anchor boxes at each position of a 3-D feature map. The Fig. 2(b) illustrates a pre-defined anchor tube at a position of a 4-D feature map. Similar to the main goal of the anchor boxes, the anchor tubes format the network output dimensions. Consequently, our network is designed to predict the tube shape offset parameters along the temporal dimension, the confidence for each object class, and the visibility of each box in the tube.

## E Further Details on Motion Model

The proposed DMM-Net outputs encoded anchor tubes directly. However, it entails predicting numerous parameters (unless a compact encoding for the tubes is used). For instance, assume that an anchor tube contains 16 boxes. In this case, the network would need to output  $16 \times 4$  scalar values to describe the tube. To limit the output parameters, we introduce the motion function to describe these boxes in an encoded anchor tube. In our experiments, we use the quadratic function that only needs  $3 \times 4$  motion parameters to describe an encoded anchor tube. The Eq. (1) below states the relationship between the motion parameters and the ground truth tracks.

$$\begin{cases} b_{i,t}^w = a_{i,t}^w \exp(p_{11}t^2 + p_{12}t + p_{13} + \Delta^w) \\ b_{i,t}^h = a_{i,t}^h \exp(p_{21}t^2 + p_{22}t + p_{23} + \Delta^h) \\ b_{i,t}^{cx} = p_{31}a_{i,t}^w t^2 + p_{32}a_{i,t}^w t + p_{33}a_{i,t}^w + a_{i,t}^{cx} + \Delta^{cx} \\ b_{i,t}^{cy} = p_{41}a_{i,t}^h t^2 + p_{42}a_{i,t}^h t + p_{43}a_{i,t}^h + a_{i,t}^{cy} + \Delta^{cy}, \end{cases} \quad (1)$$

**Table 5.** Further results on Omni-MOT with Medium and Hard camera views and Cloudy weather conditions: The symbol  $\uparrow$  indicates higher values are better, and  $\downarrow$  implies lower values are favored.

Type	View	Camera	IDF1 $\uparrow$	IDP $\uparrow$	IDR $\uparrow$	Rcll $\uparrow$	Prcn $\uparrow$	GT $\uparrow$	MT $\uparrow$	PT $\uparrow$	ML $\downarrow$	FP $\downarrow$	FN $\downarrow$	IDs $\downarrow$	FM $\downarrow$	MOTA $\uparrow$	MOTP $\uparrow$
Test	Hard	Camera_1	35.8%	41.8%	31.3%	55.8%	74.6%	116	9	34	73	3359	7801	78	184	36.3%	73.2%
	Hard	Camera_12	32.0%	38.6%	27.3%	48.0%	67.7%	136	1	38	97	2948	6704	113	188	24.2%	70.5%
	Ordinary	Camera_9	47.7%	51.1%	44.7%	68.5%	78.3%	61	16	32	13	2398	3986	42	150	49.2%	73.5%
Train	Hard	Camera_0	44.5%	48.2%	41.4%	63.7%	74.1%	137	17	36	84	2979	4865	66	155	40.9%	75.8%
	Hard	Camera_1	30.7%	36.8%	26.3%	49.7%	69.7%	148	5	38	105	3236	7537	117	202	27.4%	73.2%
	Ordinary	Camera_5	68.9%	70.9%	66.9%	81.5%	86.3%	94	32	40	22	3443	4957	62	222	68.3%	81.1%
Average	-	-	47.0%	52.0%	42.8%	63.5%	77.3%	692	80	218	394	18363	35850	478	1101	44.4%	76.1%

where  $(a_{i,t}^{cx}, a_{i,t}^{cy}, a_{i,t}^w, a_{i,t}^h)$  is the pre-defined box (center x, center y, width, height) of  $i^{th}$  anchor tube at  $t^{th}$  frame,  $(b_{i,t}^{cx}, b_{i,t}^{cy}, b_{i,t}^w, b_{i,t}^h)$  is the box of  $i^{th}$  ground truth track at  $t^{th}$  frame,  $\{p_{11}, \dots, p_{43}\}$  represents the motion parameters of the  $i^{th}$  encoded anchor tube, and  $(\Delta^{cx}, \Delta^{cy}, \Delta^w, \Delta^h)$  is the localization error of our network output. From Eq. (1), we can see that the box center  $(b_{i,t}^{cx}, b_{i,t}^{cy})$  of the ground truth track is a quadratic function of time, while  $(b_{i,t}^w, b_{i,t}^h)$  is more a complicated function. The motion parameters are able to successfully model object motion for short time slots to generate effective tracklets.

## F Further Quantitative Results

To better evaluate our technique and putting the values reported in the paper into a better perspective, we provide further results of DMM-Net on two additional viewpoints Omni-MOT. These results are reported in Table 5. The experiments are conducted for cloudy weather conditions. The selected scenes are from Town 05 (with 230 vehicles) that are indexed 1, 9, and 12 in the dataset, where scene-1 and scene-12 are with hard camera view, and scene-9 is with ordinary camera view. Similar to the experiments in the paper, we train the network for 22 epochs and use the same evaluation matrices as used in the paper. The results show good performance of DMM-Net on the realistic dataset with accurate ground-truth. For these experiments, we observed that our network was often able to track vehicles that are fully occluded. This is a direct benefit of using motion modeling for tracking. On the flip side, we also observed a slight drift of the bounding boxes for stationary objects due to the amplification of motion caused by noisy detection. Nevertheless, this problem was never observed to cause critical problems. These observations can be verified in the videos provided on the URL links above.

## References

1. Andriluka, M., Roth, S., Schiele, B.: People-tracking-by-detection and people-detection-by-tracking. In: 2008 IEEE Conference on Computer Vision and Pattern Recognition. pp. 1–8 (2008), <https://academic.microsoft.com/paper/2138302688>
2. Caesar, H., Bankiti, V., Lang, A.H., Vora, S., Liong, V.E., Xu, Q., Krishnan, A., Pan, Y., Baldan, G., Beijbom, O.: nuscenes: A multimodal dataset for autonomous driving (2019)
3. Dosovitskiy, A., Ros, G., Codevilla, F., Lopez, A., Koltun, V.: CARLA: An Open Urban Driving Simulator. In: Proceedings of the 1st Annual Conference on Robot Learning. pp. 1–16 (2017), <http://arxiv.org/abs/1711.03938>
4. Ferryman, J., Shahrokni, A.: PETS2009: Dataset and challenge. In: Proceedings of the 12th IEEE International Workshop on Performance Evaluation of Tracking and Surveillance, PETS-Winter 2009 (2009). <https://doi.org/10.1109/PETS-WINTER.2009.5399556>
5. Geiger, A., Lenz, P., Urtasun, R.: Are we ready for autonomous driving? the KITTI vision benchmark suite. In: Proceedings of the IEEE Computer Society Conference on Computer Vision and Pattern Recognition. pp. 3354–3361 (2012). <https://doi.org/10.1109/CVPR.2012.6248074>
6. Leal-Taixé, L., Milan, A., Reid, I., Roth, S., Schindler, K.: MOTChallenge 2015: Towards a Benchmark for Multi-Target Tracking. arXiv:1504.01942 [cs] pp. 1–15 (2015), <http://arxiv.org/abs/1504.01942>
7. Liu, W., Anguelov, D., Erhan, D., Szegedy, C., Reed, S., Fu, C.Y., Berg, A.C.: SSD: Single shot multibox detector. ECCV **9905 LNCS**, 21–37 (2016). [https://doi.org/10.1007/978-3-319-46448-0\\_2](https://doi.org/10.1007/978-3-319-46448-0_2)
8. Milan, A., Leal-Taixé, L., Reid, I., Roth, S., Schindler, K.: MOT16: A Benchmark for Multi-Object Tracking. CoRR **abs/1603.0** (2016), <http://arxiv.org/abs/1603.00831>
9. Sun, P., Kretschmar, H., Dotiwalla, X., Chouard, A., Patnaik, V., Tsui, P., Guo, J., Zhou, Y., Chai, Y., Caine, B., Vasudevan, V., Han, W., Ngiam, J., Zhao, H., Timofeev, A., Ettinger, S., Krivokon, M., Gao, A., Joshi, A., Zhang, Y., Shlens, J., Chen, Z., Anguelov, D.: Scalability in perception for autonomous driving: Waymo open dataset (2019)
10. Wen, L., Du, D., Cai, Z., Lei, Z., Chang, M.C., Qi, H., Lim, J., Yang, M.H., Lyu, S.: UA-DETRAC: A New Benchmark and Protocol for Multi-Object Detection and Tracking (2015), <http://arxiv.org/abs/1511.04136>